Acta Biomaterialia 137 (2022) 331–345

Contents lists available at ScienceDirect

Acta Biomaterialia

journal homepage: www.elsevier.com/locate/actbio

Full length article

Reduced thrombogenicity of surface-treated Nitinol implants steered by altered protein adsorption

Katharina Gegenschatz-Schmid[a], Stefano Buzzi[b], Jonas Grossmann[c,d], Bernd Roschitzki[c], Riccardo Urbanet[a], Roman Heuberger[e], Dorothea Glück[f], Arik Zucker[b], Martin Ehrbar[a,*]

[a] Department of Obstetrics, University and University Hospital of Zurich, Laboratory for Cell and Tissue Engineering, Schmelzbergstrasse 12, PATHG 48, Zurich 8091, Switzerland
[b] Qvanteq AG, Zurich, Switzerland
[c] Functional Genomics Center Zurich, University of Zurich/ETH Zurich, Switzerland
[d] SIB Swiss Institute of Bioinformatics, Lausanne, Switzerland
[e] RMS Foundation, Bettlach, Switzerland
[f] Blood Transfusion Service SRC, Zurich, Switzerland

ARTICLE INFO

Article history:
Received 26 April 2021
Revised 11 October 2021
Accepted 13 October 2021
Available online 19 October 2021

Keywords:
Antithrombogenic treatment
Hemocompatibility
Cardiovascular devices
Intrinsic coagulation pathway
Proteomics

ABSTRACT

Blood-contacting medical implants made of Nitinol and other titanium alloys, such as neurovascular flow diverters and peripheral stents, have the disadvantage of being highly thrombogenic. This makes the use of systemic (dual) anti-platelet/anticoagulant therapies inevitable with related risks of device thrombosis, bleeding and other complications. Meeting the urgent clinical demand for a less thrombogenic Nitinol surface, we describe here a simple treatment of standard, commercially available Nitinol that renders its surface ultra-hydrophilic and functionalized with phosphate ions. The efficacy of this treatment was assessed by comparing standard and surface-treated Nitinol disks and braids, equivalent to flow diverters. Static and dynamic (Chandler loop) blood incubation tests showed a drastic reduction of thrombus formation on treated devices. Surface chemistry and proteomic analysis indicated a key role of phosphate and calcium ions in steering blood protein adsorption and avoiding coagulation cascade activation and platelet adhesion. A good endothelialization of the surface confirmed the biocompatibility of the treated surface.

Statement of significance

Titanium alloys such as Nitinol are biocompatible and show favorable mechanical properties, which led to their widespread use in medical implants. However, in contact with blood their surface triggers the activation of the intrinsic coagulation cascade, which may result in catastrophic thrombotic events. The presented results showed that a phosphate functionalization of the titanium oxide surface suppresses the activation of both coagulation cascade and platelets, avoiding the subsequent formation of a blood clot. This novel approach has therefore a great potential for mitigating the risks associated to either thrombosis or bleeding complications (due to systemic anticoagulation) in patients with cardiovascular implants.

© 2021 The Authors. Published by Elsevier Ltd on behalf of Acta Materialia Inc.
This is an open access article under the CC BY-NC-ND license
(http://creativecommons.org/licenses/by-nc-nd/4.0/)

1. Introduction

Several different biomedical devices are currently used to treat cardiovascular diseases and need to be blood compatible due to their exposure to blood. Many of these devices consist of titanium or its alloys, such as TAV (titanium aluminum vanadium alloy) or Nitinol (nickel titanium alloy with approximately equal atomic percentages of the two elements), exploiting their good mechanical properties and corrosion resistance. In particular, Nitinol with its outstanding elasticity enables the design of devices for minimally invasive implantation techniques, which would be difficult to achieve with other materials. It is therefore widely used for endovascular stents, aneurysm treatment devices such as neurovascular flow diverters, structural heart devices or cages for heart valves. However, when titanium alloys are brought in contact with blood,

* Corresponding author.
E-mail address: martin.ehrbar@usz.ch (M. Ehrbar).

https://doi.org/10.1016/j.actbio.2021.10.022
1742-7061/© 2021 The Authors. Published by Elsevier Ltd on behalf of Acta Materialia Inc. This is an open access article under the CC BY-NC-ND license (http://creativecommons.org/licenses/by-nc-nd/4.0/)

they strongly initiate thrombus formation and inflammation. While these surface-induced effects are of advantage for osseo-integrating implants [1–3] they represent a significant challenge for cardiovascular implants [4,5]. To avoid major adverse clinical events after their implantation, the use of systemic (dual) anti-platelet and/or anticoagulant therapy is inevitable. This may increase the risk of bleeding complications, especially in elderly patients or patients that are already prone to high bleeding risks. Moreover, variable responses to anticoagulation therapy due to poor adherence to medication intake or genetic variability are inherent risks. Furthermore, especially in aneurysm treatment a fine balance between the risks of device thrombosis and aneurysm rupture is required [6,7], and this dilemma will further accentuate in the future with ageing population often having multiple implants. Reducing the needed anticoagulation during and after implantation of vascular devices would therefore be a major improvement and yet unmet clinical need.

Thrombus formation on devices results from hemodynamic alterations by the implant and/or blood-surface interactions and is driven by the adhesion and activation of both plasma proteins and platelets. Rapid adsorption of plasma proteins, such as fibrinogen and von Willebrand factor (vWF), mediate platelet adhesion through binding with their GPIIb/IIIa receptors (also known as ITGA2B and ITGB3) [8]. The initiating step in contact activation of the intrinsic coagulation pathway is the adsorption of coagulation factor XII (FXII) to the negatively charged surface and its subsequent change in conformation and autoactivation, resulting in the activated FXIIa [9,10]. Activated plasma kallikrein (PKK) and kininogen-1, also known as high molecular weight kininogen (HMWK), facilitate this activation. Then, FXIIa activates FXI in a HMWK-dependent manner, which initiates a series of proteolytic reactions involving the subsequent activation of FIX and FX and culminating in thrombin generation. Finally, activated thrombin converts fibrinogen to fibrin, which forms a clot comprising activated platelets. While this description reflects only a simplified overview, it is known that several activated coagulation factors are able to activate themselves or other factors in feedback loops. Furthermore, the activation of the coagulation cascade is highly interlinked with the activation of the complement cascade, and adhesion and activation of platelets and leukocytes.

There are several approaches to improve the blood compatibility of the surface of endovascular implants. Hemodynamic alterations by the implant can be approached by optimizing implant design such as in reducing strut diameter for stents. Blood-surface interactions depend on the implant surface chemistry and topography. While surface passivation, electro-polishing and annealing only marginally improve thrombogenicity [11–13], this can be successfully addressed by surface functionalization. A major leap forward for the endovascular treatment of intracranial aneurysms has been the development of antithrombotic coatings (reviewed in [7]). Bioactive coatings, in particular heparin-based, have shown good results for temporary applications such as extracorporeal tubing, but they have not found clinical application in the neurovascular field yet [7,14]. In this field, coatings are mainly going in the direction of hydrophilic and/or phosphate-containing coatings, in particular phosphorylcholine (PC) [7,15]. However, many coatings are of limited value for deformable implants, as they may crack or delaminate due to mechanical impacts during implant crimping, loading, or implantation and lead to exposure of the underlaying thrombogenic material.

Here, we aimed at generating a simple surface functionalization alternative to the existing coatings combining their strengths and being stable towards mechanical deformation. We hypothesized that the phosphate group is the key element for the efficacy of the PC coating and that its antithrombogenic effect is boosted by surface hydrophilicity, which is known to reduce adsorption and denaturation of blood proteins [16,17]. Indeed, the presence of phosphate can greatly affect protein adsorption to numerous surface types [18–21]. On titanium oxide (TiO_2), phosphate adsorption was not only shown to reduce albumin adsorption by 50% [18], but adsorbed phosphate could also reduce the amount of BSA denaturation on TiO_2 [21]. Both, protein quantity and conformation are key factors for the surface-induced blood coagulation [22–26]; in particular, the change of conformation of surface-adsorbed albumin was directly correlated with platelet adhesion [27].

Instead of using an organic hydrophilic coating, here Nitinol implants are directly made highly hydrophilic by removing any surface contamination, which is replaced by phosphate ions. We show that our treatment, a combination of oxide plasma treatment, and phosphate functionalization, results in ultra-hydrophilic Nitinol implants. Treated Nitinol disks and braids, when tested in static and dynamic human blood flow models *in vitro*, show a significantly reduced thrombogenicity. Proteomic and biochemical analysis indicate that this effect on treated Nitinol surface is due to a change in blood protein adhesion and a reduced initiation of blood protein contact activation.

The surface functionalization described here can be combined with a seal to protect the surface characteristics during storage. This may be required to use the technology in a medical device.

2. Materials and methods

2.1. Sample preparation

Nitinol samples with two different shapes and surface finishes were used in this study; electropolished Nitinol disks (ø14 mm, thickness 0.5 mm, Memry Corporation, USA) and Nitinol braids with thermal oxide surface finish (Blue Oxide, ø5.5 mm, filament diameter ø35 or 60 µm, Admedes GmbH, Germany). The braids were cut to proper length (6 or 15 mm).

All samples were cleaned by performing an ultrasound bath series of 10 min in 4% Deconex PA 12 (Borer Chemie AG, Switzerland), 2 × 5 min in water for injection (Laboratorium Dr. G. Bichsel AG, Switzerland), 5 min in 4% Deconex Surfax (Borer Chemie AG, Switzerland), 3 × 5 min in water for injection, 5 min in acetone 99.8% (Merck Millipore, Germany), 5 min in isopropanol 99.8% (Merck Millipore, Germany) and dried by blowing with nitrogen 5.0 under cleanroom conditions. Samples with these preparation steps were used as controls and prior to contacting blood or blood plasma they were rinsed with 0.9% saline solution (Laboratorium Dr. G. Bichsel AG, Switzerland) simulating device flushing (to remove air bubbles) in clinical applications. These samples are called Standard (S) in this manuscript (for “Standard of care”) and are marked in red in the figures.

Additionally to the above described cleaning procedure, some samples were prepared with a surface finish which involves two steps. First, an oxygen plasma treatment (PDC-002, Harrick Plasma, USA, using a pressure of 8×10^{-3} mbar and oxygen 99.995%) to remove any organic surface contaminants and to activate the surface for further functionalization. Second, a phosphate functionalization of the surface by immersing in a 100 mM aqueous solution of KH_2PO_4 (1.04873.1000, Merck KGaA, Germany, dissolved in water for injection, Laboratorium Dr. G. Bichsel AG, Switzerland) for hemocompatibility. To simplify handling, most samples were sealed with a fast soluble carbohydrate essentially acting as packaging layer which protects the ultra-hydrophilic and functionalized device surface during packaging, sterilization, storage and transportation. The sealing consisted of trehalose (T104-4, Pfanstiehl GmbH, Switzerland), applied in form of a 50 mM aqueous solution (in water for injection, Laboratorium Dr. G. Bichsel AG, Switzerland) and dried overnight at 30°C, but other mono- and disaccha-

rides such as glucose (2057553, Laboratorium Dr. G. Bichsel AG, Switzerland) were successfully tested as well (data not shown). The sealing immediately dissolves upon immersion in physiological solutions or blood, exposing the functionalized Nitinol surface; it does not play any active role in the blood-surface interaction. These samples were rinsed with simulated body fluid (Hanks' solution, H8264-500ML, Sigma-Aldrich, UK) to remove the sealing prior to blood contact. For simplicity, the term simulated body fluid is also referred to as SBF from now on. These samples are called Treated (T) and are marked in blue in the figures.

2.2. Surface analysis

Static water contact angle was visualized by placing 3 µl of water for injection on the disks and taking a side shot of the droplet immediately thereafter for angle assessment. For treated disks, the measurement was performed after removing the protecting sealing layer by rinsing with water for injection and drying by nitrogen blowing.

The surface chemistry was analyzed by X-ray photoelectron spectroscopy (XPS). Standard and treated disks were rapidly immersed three times in the respective flushing solutions and then immersed three times in water for injection and blow-dried with nitrogen (99.998%) before placing on the XPS sample holder. A Kratos Axis Nova spectrometer was used (Kratos Analytical, UK), with a 225 W monochromatic Al Kα radiation on an area of 700 x 300 μm. The photoelectrons were detected with a hemispherical analyzer at a takeoff angle of 90° with a pass energy of 40 eV (0.1 eV step size, fwhm ($Ag3d_{5/2}$) = 0.6 eV). The peak fitting was performed with the CasaXPS software (V2.3.17, Casa Software Ltd., UK) after subtracting an iterated Shirley background. To quantify the surface composition, the areas of the peaks were corrected by the sensitivity factors given by Kratos. Peak shifting was corrected by referencing the aliphatic carbon peak (from residual contamination) to 285 eV. The thickness of the oxide film was calculated using the Hill-equation [28]. The roughness of the sample was taken into account according to Gunter et al. [29,30], taking a correction factor of 0.88 for technical surfaces. The uncertainty is about 25% of the reported thickness values.

2.3. Whole blood incubation tests

Human blood was obtained from healthy volunteer donors (ethical approval University Hospital Zurich, Switzerland: KEK-ZH 2012-0302) who had not used medication in the previous 2 weeks. Blood was drawn in 5 ml vacutainer tubes (367614, BD, Switzerland) and supplemented with 50 µl of 50 IU/ml or 300 IU/ml heparin (Heparin-Na 25'000 I.E./5 ml, B. Braun AG, Switzerland), diluted with phosphate buffered saline (PBS, 10010-015, Thermo Fisher Scientific, USA), to reach a final concentration of 0.5 IU or 3 IU heparin per ml blood. Freshly drawn blood (not older than 30 min) was used in all experiments. Hemocompatibility evaluations were performed according to ISO 10993-4 [31].

For tests with disks, 24-well plates (92024, TPP, Switzerland) with 1 ml of blood were used; for static blood incubation with braids, tests were performed with 2 ml of blood in cryotubes (89012, TPP, Switzerland). Incubation was performed at 37 °C for 1 h under static conditions (cryotubes reversed and well plates rapidly agitated every 10 min to avoid cell sedimentation).

For dynamic blood incubation tests with braids, a Chandler loop setup [32] with up to 6 parallel loops was used (Ebo kunze industriedesign, Germany). Braids were deployed in 4.75 mm PVC NoDOP tubes (Raumedic, Germany) with a length of 50 cm. The tubes with braids were filled with 7.1 ml of fresh blood (corresponding to 80% of the loop volume) and closed, forming a round loop. The loops rotated with 30 rotations/min at 37 °C for 1 h (blood flow rate ~210 ml/min). Blood was then filtered (Falcon 70 µm cell strainer, Corning, USA) for visualizing potential free-floating thrombi, and plasma aliquots were collected for subsequent analysis (transfer of 4.5 ml of blood into CTAD vacutainers (367599, BD, Switzerland), cooling in iced water for 15 min, double centrifugation (1500 g + 2500 g) for 20 min at 4 °C with collection of upper plasma portions, stored at -80 °C until measurement). Devices were extracted from the loops with tweezers, rinsed 9 times in PBS and fixed for 1 h in 4% paraformaldehyde (Artechemis, Switzerland). Macroscopic pictures of the samples were shot. In addition, selected samples were stained for fluorescence microscopy imaging (DM550B, Leica Microsystems, Germany) with the following combination of stainings and dilutions in PBS: Hoechst (1:1000, H3570, ThermoFisher, USA), CD41 (1:200, ab134131, Abcam, UK + 1:500, AlexaFluor® 568 anti-rabbit, ab175471, Abcam, UK) and Fibrin (1:500, F9902, Sigma Aldrich, USA + 1:1000, Alexa Fluor® 488 anti-mouse, ab150113, Abcam, UK). Finally, adherent human blood components were investigated by scanning electron microscopy (SEM). Samples were fixed for 30 min in 2.5% glutaraldehyde in PBS, dehydrated in a graded series of ethanol (from 20% to 100% in water), followed by immersion in hexamethyldisilazane (50% and 100%) and drying. The samples were sputter-coated with 3 nm platinum, and the images were recorded using a Leo 1530 SEM (Zeiss, Germany) using an InLens detector and 5 kV acceleration voltage.

Activation of coagulation cascade and platelets were quantified by measuring the concentrations in blood plasma of thrombin-antithrombin complex (TAT) and β-Thromboglobulin (β-TG), respectively. ELISA kits were used (TAT: Enzygnost TAT micro, OWMG15, Siemens Healthineers, Germany; β-TG: Asserachrom β-TG, 00950, Stago, France).

2.4. Blood protein adsorption and peptide preparation

Blood was collected analogously to what described above for whole blood incubation tests, anticoagulated with 3 IU/ml heparin to enable longer manipulation. Platelet-poor plasma (PPP) was collected after two rounds of 15 min centrifugation at 1200 g and at room temperature (RT).

Nitinol disks were inserted into a 24-well plate (92024, TPP, Switzerland). 0.5 ml of PPP were added to each well and the samples were incubated at 37°C for 1 h. Standard and treated disks were incubated each with PPP of three different donors. After incubation, the Nitinol surfaces were washed 3 times with PBS prior peptide preparation.

For protein digestion and peptide elution from Nitinol disks, the surfaces were incubated with 400 µl 1 M Urea in 0.1 M tris buffer (pH 8.5). Tris-(2-carboxyethyl)-phosphin (TCEP) was added to reach a final concentration of 5 mM and incubated for 30 min at RT. After that, chloroacetamide (CAA) was added to reach a final concentration of 15 mM and the samples were further incubated for 20 min at RT. Proteins were digested overnight at 37 °C with trypsin (Promega, Madison, WI), in a trypsin to protein ratio of 1:10. Trypsin activity was stopped with addition of 20 µl of 10% formic acid (FA). Eluted peptides were then desalted using self-made stage tips packed with reverse phase C18 material as follows [33]: After a first wetting step with 150 µl 100% methanol and centrifugation for 1 min at 2000 g, the tips were cleaned with 150 µl 60% acetonitrile (ACN)/0.1% trifluoroacetic acid (TFA) for 1 min at 2000 g. Prior sample loading, the tips were equilibrated twice with 150 µl 3% ACN / 0.1% TFA for 1 min at 2000 g. After sample loading of 150 µl, tips were centrifuged for 1.5 min at 2000 g and this step was repeated until full loading of the sample. After that, the tips were washed twice with 150 µl 3% ACN / 0.1% TFA for 1 min at 2000 g. Desalted peptides were eluted in total 160 µl, by adding twice 80 µl 60% ACN / 0.1% TFA and centrifuging 2 min at 2000 g.

Samples were dried to completeness by vacuum centrifugation and peptides were resolved in 20 µl mass spectrometry (MS) buffer (3% ACN / 0.1% FA) prior sonication for 5 min.

2.5. NanoUPLC-MS/MS measurements

Prior injection, peptides were further diluted with MS buffer in a ratio of 1:10 to a final volume of 15 µl including 1.5 µl iRT peptides for internal retention time normalization and quality control (Ki-3002-1, Biognosys, Switzerland). Additionally, a pool of these samples was prepared by mixing 1 µl of each sample in a new vial. The samples were analyzed with the high field orbitrap benchtop mass spectrometer Q Exactive HF (Thermo Fisher Scientific, Germany) coupled to a nano Ultra Performance Liquid Chromatography (UPLC, Aquity UPLC M-Class, Waters Corporation, USA) at the Functional Genomic Center in Zurich (FGCZ). Injection of the samples was done in randomized order with a controlled standard QC sample after every 7th sample for quality control. The samples were loaded onto a Symmetry C18 trap column (5 µm, 75 µm X 250 mm, Waters Corporation, USA) and eluted at a flow rate of 300 nl/min on a HSS T3 C18 reverse-phase column (1.8 µm, 75 µm X 250 mm, Waters Corporation, USA). Solvent composition of mobile phase A was 0.1% FA in ddH_2O and of mobile phase B was 0.1% FA in ACN. The peptides were separated with the following LC gradient: 0-49 min 8-22% B, 49-60 min 22-32% B, 60-65 min 95% B, 65-75 min: 8% B.

Full mass spectra were acquired in the m/z range of 300-1700, at a resolution of 120000 at 200 m/z, with an automatic gain control (AGC) target of 3e6 and a maximum injection time of 50 ms. MS/MS spectra were acquired in a scan range of 200-2000 m/z, at a resolution of 30,000 at 200 m/z, AGC target at 1e5 and a maximum injection time of 55 ms. The 12 most abundant ions were selected for higher energy collision dissociation (HCD) with a normalized collision energy of 28, and an isolation window of 1.6 m/z. Precursor masses already selected for MS/MS acquisition were excluded from further selection for 30 s. Furthermore, unassigned, single charged precursors and precursors with charges higher than +8 were excluded and intensity threshold was set to 8.2e4.

2.6. Protein identification and web-based protein set analysis

The raw mass spectrometry (MS) files were imported into the ProgenesisQI for proteomics software (Waters Corporation, USA). Automatic alignment after manual seeding increased the alignment score to > 90% for all files. Peptide ions were filtered for positive charges of +2, +3 and +4. For peptide identification, the 5 highest ranked MS/MS spectra with a limit ion fragment count of 200 were exported using charge deconvolution and deisotoping. The generated mascot generic file (.mgf) was searched with Mascot Server 2.6 (Matrix Science Ltd, UK) allowing two missed cleavages by trypsin and using the following parameters: carbamidomethylation of cysteine as fixed modification, oxidation on methionine and deamidation of asparagine and glutamine as variable modifications, 10 ppm peptide mass tolerance, 15 ppm MS/MS tolerance, and the value for number of ^{13}C set to 1. We searched the canonical human reference proteome (only reviewed proteins) as forward and concatenated to its reversed entries and known mass spectrometry contaminants (downloaded in December 2016). The mascot results were then imported into Scaffold (v4.8. Proteome Software, Inc., USA). The spectrum report was exported using the filters of 10% protein false discovery rate (FDR), minimum 1 unique peptide and 5% peptide FDR. The exported file was reimported into the ProgenesisQI for proteomics software for further processing. The protein hits were normalized using the set of iRT peptides as normalization factors. For quantification prior export of protein and peptide lists in excel format, relative quantitation using Hi-N with 3 peptides was selected [34]. Protein hits were further filtered for minimally 2 peptide count and 2 unique peptides resulting in a protein list of 232 proteins with a FDR of <1%. After elimination of decoy proteins, non-human contaminants and iRTs, a list of 224 protein hits remained. The mass spectrometry proteomics data have been deposited to the ProteomeXchange Consortium via the PRIDE [35] partner repository with the dataset identifier PXD024284.

To identify and categorize individual proteins out of the 224 protein-comprising hit list with specific function in the blood coagulation pathway and/or complement cascade, over-representation analyses (ORA) were performed with the web-based tool WebGestalt (webgestalt.org) [36]. As functional reference databases served Wikipathway (wikipathway.org), panther pathway (pantherdb.org) and KEGG pathway (genome.jp/kegg/pathway) with searching in the category “pathway” and against the human protein-coding genome. For identification of the enriched categories all ORA analyses were performed with the default search settings: Number of 20–500 genes per category, multiple test adjustment using Benjamini–Hochberg correction, and using top 10 most significant categories and expecting 10 categories from set cover.

2.7. Static blood incubation tests with FX(a) pre-coated braids and factor X and XII inhibitors

Prior incubation with blood, selected braids were coated with FX in its active or inactive form. For this, 2 ml test tubes were first passivated with 2 ml SBF containing 0.1 mg/ml bovine serum albumin (BSA, A2153-50g, Sigma-Aldrich, USA) for 30 min. The BSA/SBF was then removed and 500 µl of 50 nM or 200 nM native human FX (inactive form, ab62549, Abcam, UK) and native human FXa (active form, ab62229, Abcam, UK) in SBF were added. Standard and treated braids (5.5 × 6 mm in size) were pre-incubated in the protein/SBF for 1 h at RT, then they were shortly washed in SBF to remove non-adhering proteins and transferred into 2 ml tubes containing 0.5 IU/ml heparinized blood. For factor FX and FXII inhibition, heparinized blood (0.5 IU/ml) was further supplemented with Rivaroxaban (FXa inhibitor, BAY 59-7939, 16043, Cayman Chemical, USA) to final concentrations of 1-25 µg/ml or with FXII900 (Factor XIIa inhibitor, EPFL, Switzerland) to a final concentration of 1–100 µM [37]. Static blood incubation tests were then performed as described above.

2.8. Measurement of endothelialization on Nitinol disks

GFP-expressing Human Umbilical Vein Endothelial Cells (HUVECs) at passage 9 (PEL-PB-CAP-0001GFP, Abc biopply AG, Switzerland) were initially expanded on a T75 flask with EGM-2 medium (CC-3162, Lonza, Switzerland). Once cells reached a confluence around 70%, they were trypsinized and resuspended at a final concentration of 50k cells/ml. Standard and treated disks were placed in a 24-well plate (92024, TPP, Switzerland) and 500 µl of cell suspension was added on top. After 2 h of incubation, the cell suspension was aspirated, the disks were placed in a 30 mm-culture dish (93040, TPP, Switzerland) and the entire excessive medium around the disk was aspirated allowing the disk to vacuum-adhere to the plastic surface. 2 ml of fresh EGM-2 were added to the cultured disks and the medium was further changed every day. Picture acquisition occurred immediately after the disk transfer (0h) and at 24, 48 and 96 h of culture. The images were taken with an upright fluorescence microscope (DM5500-B, Leica, Switzerland) at 25x magnification. Five standard and 5 treated disks were tested; cell coverage was quantified by applying a fixed threshold for the

fluorescence signal on 5 independent pictures per disk and calculating the area percentage covered with cells using Fiji software [38].

2.9. Statistical analysis

XPS-based concentrations of surface elements were compared with an unpaired two-tailed Student's t-test assuming a normal distribution; probabilities $p \leq 0.05$ were considered as significant.

Statistical analysis of TAT and β-TG activation by ELISA as well as of the cell coverage on nitinol disks was performed by two-way ANOVA analysis accepting significance for $p \leq 0.05$ after comparing the mean values by Bonferroni post hoc test. Significance is designated by an asterisk. p-Values of the protein hits from MS were calculated using a two-tailed paired t-test function on the hyperbolic arcsine of the normalized values. Fold changes (FCs) were calculated using the logarithmic transformation (base 2) of the mean-normalized values. Only protein hits with p-values ≤ 0.05 and a cutoff at $FC > 2$ ($= \log2(T \text{ vs } S) > 1$) were considered as significant.

All statistical evaluations were performed in Excel (Version 16.50).

3. Results

3.1. Surface functionalization aiming for increased and stable hydrophilicity

To reduce the thrombogenic properties of Nitinol stents, we aimed at forming a highly hydrophilic surface and developed a surface treatment which includes the removal of organic contamination and its subsequent functionalization with phosphates. To characterize the effect and stability of the treatment on the hydrophilicity of the surface, small droplets of water were applied on standard and treated disks one month after treatment, with storage at ambient conditions. Contact angle measurements revealed that standard surfaces are mildly hydrophobic with a contact angle between 70° and 90°. In contrast, surface-treated samples were highly hydrophilic with a contact angle of $\leq 10°$ (Fig. 1).

Next, to determine the effect of the treatment on the chemical composition of the surface, XPS measurements were conducted on standard and treated disks. Based on the areas below the peaks, a quantification of the composition of the oxide layer of the disks was performed and the thickness of the oxide was estimated based on the amount of detected oxidic and metallic bonds of Ti and Ni (Table 1). Both standard and treated surfaces had an oxide layer consisting of titanium oxide (>97%) with only traces of nickel oxide ($p = 0.09$). The oxide layer of treated disks was slightly thicker and increased concentrations of phosphorus (in form of phosphate, P2p3/2 peak at a binding energy of 133.5 ± 0.5 eV). In addition, small amounts of calcium and magnesium were detected which likely originate from the rinsing step in SBF ($p < 0.01$ for all). The Ca/P atomic ratio of 0.43 is far away from the ratio (1.67) of hydroxyapatite, which would be the most stable form of calcium phosphate at blood pH [39]. This is in line with published results of Nitinol and titanium incubation in Hanks' solution [40] and substantiates the equilibrium of this layer with the surrounding liquid without precipitation or induced nucleation [41].

In both standard and treated cases the ratio of O : (Ti_{ox}+ Ni_{ox}) was 2.9 : 1. This was more than the expected 2 : 1 for TiO_2, indicating that part of the oxygen originated from above the metal oxide layer (phosphates, hydroxides, adsorbed water, organic compounds, potentially calcium and/or magnesium oxides). Instead, no noteworthy increase of phosphorus, calcium and magnesium was detected on standard surfaces rinsed with SBF instead of using the standard saline solution (Suppl. Table 1). Finally, treated surfaces showed a tendency to a lower concentration of hydrocarbons ($p = 0.19$). Together, treated surfaces were highly hydrophilic and contained phosphates, while standard surfaces were hydrophobic and did not contain phosphates.

Fig. 1. Water wettability of Nitinol disks: Standard (S, top) and treated (T, bottom) disks with a water droplet placed on the center.

Table 1
Surface composition determined by XPS. The ratios were normalized by titanium and nickel in the oxide layer.

		Ti_{ox}	Ni_{ox}	O	P	Ca	Mg	C	d_{ox} [nm]
Standard	average	0.99	0.01	2.9	0.03	0.00	0.00	1.9	5.5
	st.dev	0.00	0.00	0.4	0.01	0.00	0.00	0.8	0.1
Treated	average	0.97	0.03	2.9	0.14	0.06	0.05	0.8	6.3
	st.dev	0.01	0.01	0.0	0.01	0.00	0.00	0.0	0.1

St.dev = standard deviation; d_{ox} = estimated oxide layer thickness.

3.2. Nitinol treatment is stable over time and reduces blood coagulation response in static incubation tests

To dissect the impact and longevity of Nitinol treatment on thrombogenicity, we performed static blood incubation tests. For that, standard and treated disks and braids were incubated statically for one hour in fresh human blood containing different concentrations of the anticoagulant heparin. With relatively high concentration of heparin (3.0 IU/ml), early stages of clotting can be observed, while addition of low concentration of heparin (0.5 IU/ml) enables observing advanced, later clotting stages. At early stages, neither standard nor treated samples showed a macroscopic thrombus. However, investigations by fluorescence microscopy and SEM showed platelet adhesion and formation of fibrin fibers on standard samples, concentrated in small "islands" partially interconnected by single fibers with each other and platelets. Platelets showed generally a flat round shape but, in contact with fibers, they often had pseudopods. Treated disks had instead only nucleated cells on the surface (Fig. 2).

With decreased concentrations of heparin (0.5 IU/ml), and therefore advanced clotting stages, macroscopically clearly visible blood thrombi formed on both standard disks and braids. Microscopic examinations revealed dense networks of fibrin fibers that also contained trapped platelets and other blood cells. In contrast, in the same low anticoagulation condition treated disks and braids appeared macroscopically clean and with metallic appearance. The treated surfaces were free from fibrin fibers and had only a few adhering platelets. Nucleated cells, mainly neutrophils based on the nuclear morphology, were present independently of the surface treatment. Summarized, the surface treatment drastically reduced thrombus formation macroscopically and microscopically under static conditions.

In order to examine the usability of the technology for medical devices we tested treated and sealed surfaces after sterilization with radiation or ethylene oxide and after aging (Suppl. Fig. 1A). Also, direct immersion (without prior flushing with SBF) and direct blood testing after functionalization showed that sealing has no impact on thrombogenicity response (Suppl. Fig. 1B).

To assess the durability of the antithrombogenic effect of treated surfaces after blood contact, treated braids were immersed in SBF for one month before subjecting them to the static blood in-

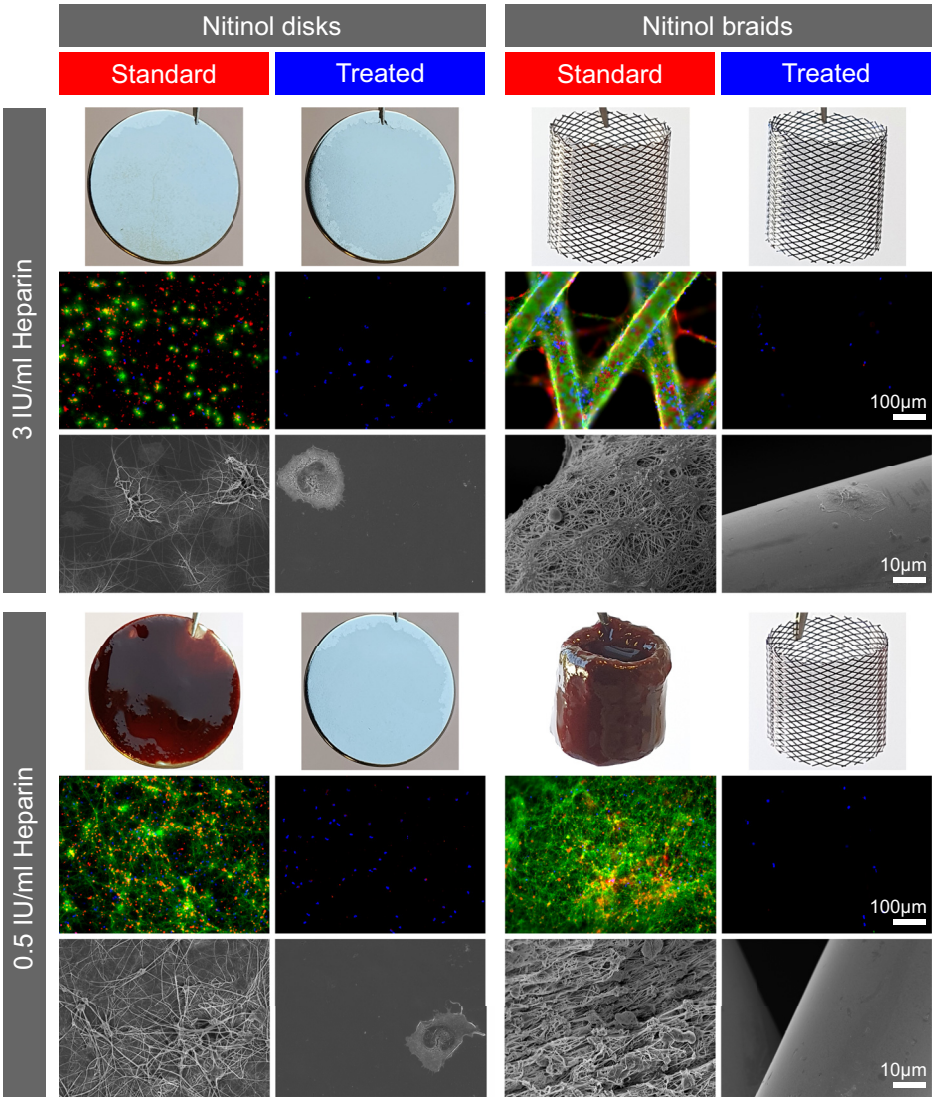

Fig. 2. Early stage (3 IU/ml heparin) and late stage (0.5 IU/ml heparin) static blood coagulation assay with standard and treated disks and braids. Macroscopic, fluorescence microscopy (blue: nuclei, red: platelets, green: fibrin) and SEM images. (For interpretation of the references to color in this figure legend, the reader is referred to the web version of this article.)

cubation test. Long pre-incubation in SBF did not change the level of antithrombotic response of treated surfaces (Suppl. Fig. 1C). In conclusion, Nitinol surface treatment is stable and reduces thrombogenicity effectively.

3.3. Reduced blood coagulation response in dynamic flow loop experiments with treated Nitinol

To test braids in an *in vitro* setting closer to the *in vivo* setup, a dynamic system mimicking blood flow, known as Chandler loop [32], has been established. Impressively, when incubating standard braids in Chandler loops containing mildly anticoagulated (0.5 IU/ml heparin) fresh human blood for 1 h, blood revealed a strong tendency to clotting. In contrast, loops with surface-treated braids and loops without a device were free of clotting (Fig. 3). In loops containing standard braids, flow irregularities due to thrombus formation were already observed after 30-45 min and in 35% of test runs the blood completely stopped circulating prior to the end of the experiment due to total thrombotic occlusion within the braids. A visual observation showed that on standard braids, thrombi formed mainly at the downstream end with protrusions exiting the braid (Fig. 3A). Additionally, free-floating pieces of thrombi could often be collected by filtering the blood after stopping the experiment. The treated braids instead showed macroscopically still a metallic appearance after the blood test and a microscopic investigation indicated adhesion of some isolated cells on the filaments and only sporadically the presence of small aggregates of cells or fibrin at filament crossings.

To confirm these visual observations, Thrombin-Antithrombin complex (TAT) formation was determined in the blood samples from Chandler loops (Fig. 3B). TAT is a widely used indicator of the coagulation cascade activation that directly correlates with thrombin concentration in the blood and fibrin mesh formation [42,43]. TAT measurements showed a massive concentration increase (>100-fold) in blood which was in contact with standard braids compared to blood with treated braids. Importantly, TAT concentrations in blood from loops which contained treated braids were not significantly increased compared to blood from loops without any devices. Analogously, the platelet activation marker β-Thromboglobulin (β-TG) was found in significantly higher concentrations (10-fold) in blood samples in contact with standard braids compared to treated braids and loops without device (Fig. 3C).

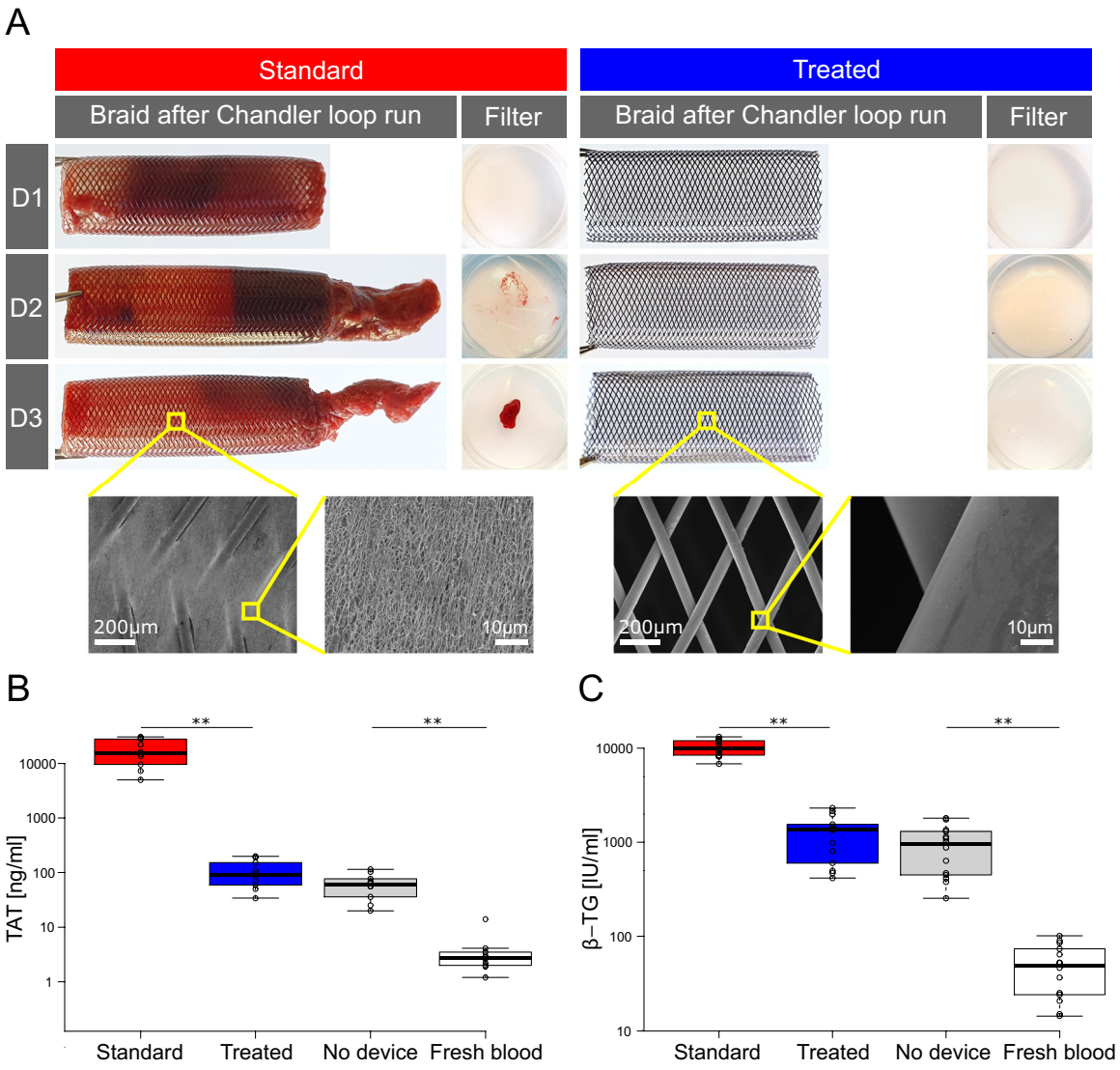

Fig. 3. Outcome of Chandler loop tests with Nitinol braids after 1 h blood flow (0.5 IU/ml Heparin). (A) Macroscopic visual observation and SEM images of devices and related free-floating thrombi (collected by filtering the blood) after 3 representative tests. (B and C) Boxplot showing (B) quantification of Thrombin-Anti-Thrombin complex (TAT) with n=10 and (C) quantification of β-Thromboglobulin (β-TG) with n=14. Center lines show the medians; box limits indicate the 25th and 75th percentiles as determined by R software; whiskers extend 1.5 times the interquartile range from the 25th to 75th percentiles. (**p < 0.001). (For interpretation of the references to color in this figure legend, the reader is referred to the web version of this article.)

3.4. Proteins of coagulation and complement cascades as well as calcium-ion binding proteins adsorb differently upon treatment

We and others have shown earlier that the blood protein coverage of stents depend on their surface properties [22–26]. It is well known that blood proteins adhere very rapidly to implant surfaces and that the protein composition layer evolves over time [44,45], also known as Vroman effect [46]. To determine the difference in protein adhesion to standard and treated surfaces, we incubated both disks in blood plasma for 1 h. Surface-adsorbed plasma proteins were trypsinized and eluted peptides were processed for mass spectrometry (MS) analysis. Protein identification and quantification was analyzed with the ProgenesisQI for proteomics software using the raw MS files. Database search of MS results revealed 5169 peptides, which were assigned to 397 proteins. After the exclusion of unique peptide ions and peptides found in more than one protein a list of 232 proteins with a FDR <1% was obtained. For further analysis, decoy proteins, non-human contaminants and iRTs were excluded, resulting in a list of 224 proteins. Out of these, 64 proteins had an increased abundance with more than 2-fold increased change on standard and 23 a higher abundance on treated surfaces (Fig. 4A). Of these proteins 78 were significant ($p \leq 0.05$ and log2(T vs S) > 1), with 58 proteins on the standard surfaces (Fig. 4A, red marks) and 20 proteins on the treated surfaces (Fig. 4A, blue marks).

To identify the individual proteins involved in the blood coagulation and the complement cascade, we performed ORA analyses in WebGestalt using the reference databases Wikipathway (wikipathway.org), Panther pathway (pantherdb.org) and KEGG pathway (genome.jp/kegg/pathway). A total of 30 proteins were classified to the blood coagulation cascade (Suppl. Table 2). Out of these, 13 proteins had significantly different abundances between standard and treated surfaces, represented in Fig. 4A–C. Comparing the individual proteins of the blood coagulation cascade, standard surfaces had a significantly higher abundance for the coagulation factors FV and FXI, for HMWK, plasminogen, carboxypeptidase B2 (CBPB2) and plasma serine protease inhibitor (IPSP, also known as SERPINA5), while to treated surfaces adsorbed with significantly higher abundance integrin β-3 (ITGB3) and all but one of the vitamin-K dependent family members. These include coag-

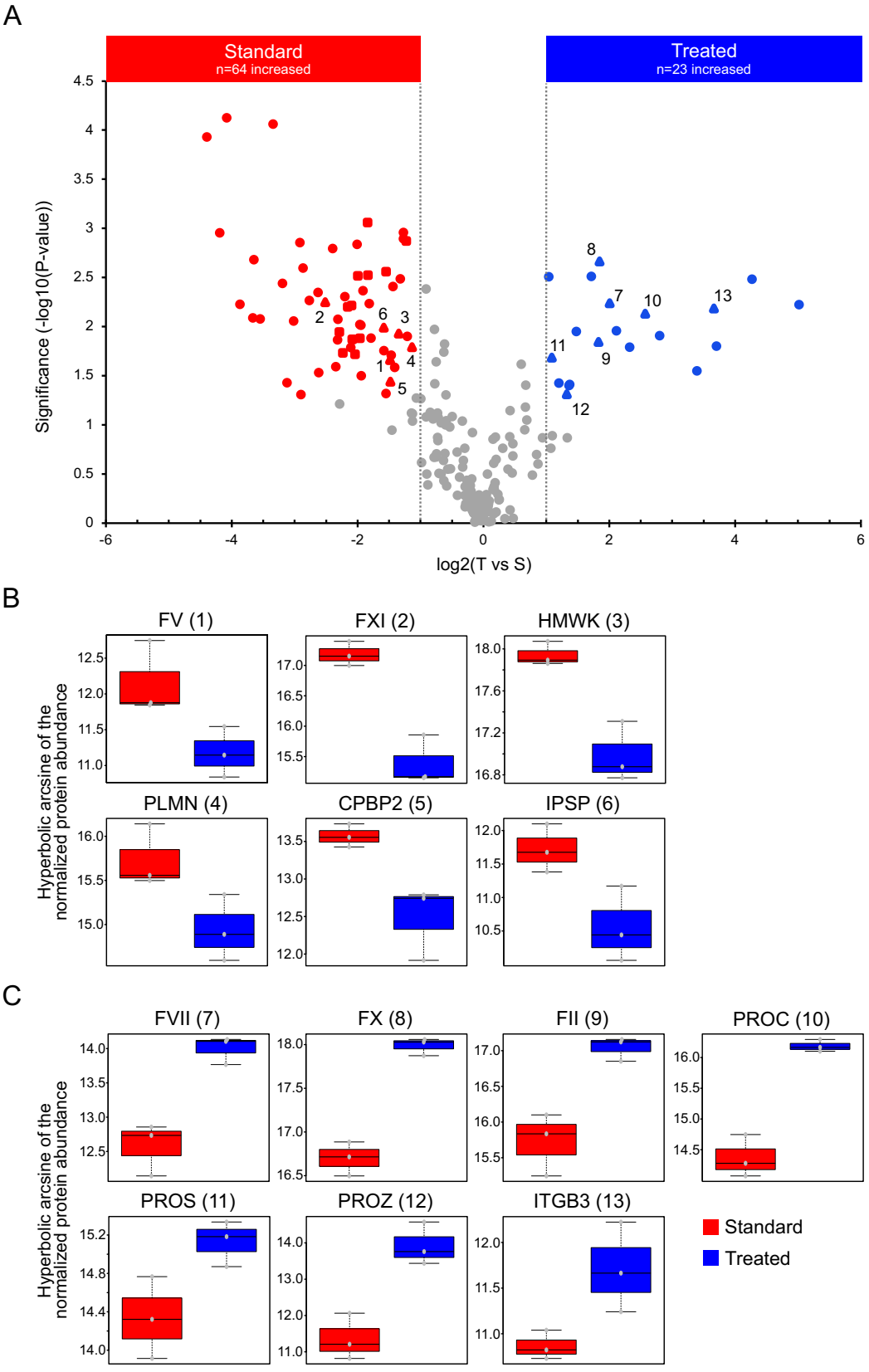

Fig. 4. Protein identification on treated vs standard Nitinol disks. (A) Volcano plot showing the significance as function of log10 (p-value) and fold change as log2 ratio of T vs S of the mean values. Significant ($p \leq 0.05$ and log2(T vs S) > 1) differentially adsorbed proteins are colored (standard in red and treated in blue). Insignificantly different proteins are marked in grey. Increased abundance was observed on standard disks for 64 proteins and on treated disks for 23 proteins. Furthermore, significant proteins participating in the blood coagulation cascade are depicted with triangles and significant proteins participating in the complement cascade with squares. Significant proteins in the blood coagulation cascade are numbered and correspond to the numbering in (B and C). (B and C) Boxplots of the hyperbolic arcsine of the normalized protein abundance of proteins of the blood coagulation cascade with significant increased abundance on standard (B, colored in red) and significantly increased abundance on treated disks (C, colored in blue). Numbering of proteins corresponds to the same in the volcano plot. (For interpretation of the references to color in this figure legend, the reader is referred to the web version of this article.)

ulation factors FVII and FX, prothrombin (FII), and the vitamin K-dependent proteins C (PROC), S (PROS) and Z (PROZ). Vitamin K-dependent proteins share the structural and functional feature of an N-terminal gamma-carboxyglutamic acid-rich (GLA)-domain allowing to bind calcium ions. Interestingly, also the twelve most abundant proteins found on treated surfaces share the capacity to bind calcium ions. These include: endoplasmin, fibroblast growth factor receptor 1 (FGFR1), FVII, FX, growth arrest-specific protein 6 (GAS6), heat shock protein HSP 90-alpha and -beta, osteopontin, PROC, PROZ, prothrombin and secretogranin 1 (see also complete protein hit list deposited to the ProteomeXchange server, PXD024284). Together with the increased abundance of the calcium-binding vitamin K-dependent coagulation factors, these results point to a selectivity for calcium-ion bound proteins on phosphate-functionalized treated surfaces.

Analyzing the identified protein hits for their function in the complement cascade, we classified 28 proteins, of which 12 were significantly different between the two compared groups (Fig. 4A and Suppl. Table 3). Out of these, all were significantly reduced on treated surfaces. The calcium ion-binding complement C1R subcomponent (C1R) protein was found with a slightly increased abundance on treated surfaces (approaching significance with p-value = 0.04 and log2(T vs S) = 0.67). Therefore, proteins of the complement pathway preferentially adsorbed to standard surfaces and surface treatment reduced their adsorption.

Together, these findings indicate that multiple coagulation- and complement-related proteins adsorbed to treated and standard surfaces with significantly different efficiency. However, the increased adsorption of selected pro-coagulating proteins (FX, FVII, prothrombin) on the non-thrombotic treated surfaces seems counterintuitive.

3.5. Activity of adsorbed FX on standard and treated Nitinol surfaces

In an earlier study, we have observed that additionally to the quantity and ratio of blood protein adhesion, the structural or functional properties of adherent proteins can be modulated by the surface properties of materials [26,47]. To test whether the treatment of Nitinol in this study induced similar effects we next aimed at determining the activity of selected surface-adherent proteins.

Active FX is the central protein of the extrinsic and intrinsic coagulation pathway, and its functionality is essential for a thrombotic outcome. And, most importantly, it adsorbed with an increased abundance on treated surfaces despite the much lower thrombogenicity showed by this surface. To elucidate if the difference in the thrombotic outcome between standard and treated is due to unequal activation or deactivation of FXa upon surface binding, we evaluated the influence of FX activity on thrombus formation. For that, standard and treated braids were pre-coated with different concentrations (50 nM and 200 nM) of either native human full-length FX or its activated form FXa prior to blood contact for 1 h. Static blood incubation tests showed that pre-adsorption with lower or higher concentrations of FX did not accelerate the blood clotting response on both standard and treated braids (Fig. 5A). Additionally, pre-coating of standard braids with FXa had no effect on blood clotting. Instead, pre-incubation of treated braids with FXa resulted in a concentration-dependent induction of blood clotting. Furthermore, inhibition of FXa activity by addition of increasing concentrations of Rivaroxaban (1, 5, and 25 ug/ml) to the blood resulted in a dose-dependent reduction of coagulation on standard braids. Together, these findings indicate that FX activation is significantly less efficient on treated surfaces than on standard surfaces or is not happening at all.

To further discern the potential mechanism of blood coagulation activation on the standard surfaces, we inhibited FXII, the initiator of the intrinsic contact coagulation pathway. Different concentrations of the specific factor FXII-inhibitor FXII900 (1, 10, and 100 µM) were added to the blood prior braid contact. FXII900 blocked standard surface-induced blood coagulation in a concentration-dependent manner (Fig. 5B), suggesting that on standard surfaces blood coagulation occurs mainly through the intrinsic FXII-mediated pathway, meaning that this pathway is not activated on treated surfaces.

3.6. Endothelialization on treated surfaces is preserved

Initial global endothelialization along the flow-diverting braid is a crucial process for facilitating aneurysm healing [48–50]. Furthermore, a good coverage of endothelial cells is linked to reduced platelet adhesion, reduced stent thrombosis and increased long-term patency [51,52]. To address this point, we performed endothelialization tests with GFP-expressing HUVECs on standard and treated disks and observed cell coverage over 4 days. Results showed no statistically significant difference in cell proliferation rate and on both surfaces > 90% coverage was reached within 4 days (Fig. 6). This indicates that endothelialization is not impaired by the surface treatment.

4. Discussion

Nitinol is a thrombogenic material which, however, features ideal mechanical properties for the manufacturing of stents and other medical devices that need to be highly flexible [4]. In this study we describe a new durable Nitinol surface treatment that, by combining surface hydrophilicity and phosphate functionalization, precludes Nitinol from unfolding its thrombogenic potential. We show that the improved blood compatibility of such Nitinol treated surfaces occurs by modifying blood protein adsorption and activation.

4.1. Blood activation in contact with standard Nitinol surfaces

In both static (Fig. 2) and dynamic chandler loop tests (Fig. 3) we observed significant adhesion and activation of platelets as well as the formation of a macroscopic thrombus on standard samples. This behavior was analogous on electropolished disks and electropolished plus thermally oxidized (blue oxide) braids (Fig. 2). However, this is not surprising because in both cases the outermost Nitinol layer consists mainly of thrombogenic titanium oxide, which rapidly forms naturally also on electropolished surfaces. Indeed, also in earlier studies the direct comparison of thermally oxidized versus standard braids showed only minimal differences in blood response [13]. Furthermore, the standard surface-induced blood coagulation through activation of the contact pathway was confirmed by its suppression with the highly specific FXIIa-inhibitor FXII900 [37] (Fig. 5B). This finding is in agreement with an earlier study that used the less specific corn trypsin inhibitor [4].

4.2. Surface-treated Nitinol with improved blood compatibility

Our approach to improve the blood compatibility of Nitinol combines the prevention of surface contaminations with hydrocarbons and the functionalization of the titanium oxide layer with phosphate ions. The preservation of very hydrophilic surface properties on stored treated disks, as shown by the low water contact angle (Fig. 1), demonstrated that carbohydrates effectively prevent the adsorption of air-born hydrocarbons and that they do not interfere with surface hydrophilicity. This combination of surface modifications resulted in a surprisingly dramatic decrease of surface-induced blood clotting on treated compared to standard samples (Figs. 2 and 3). Furthermore, this improvement was consistent

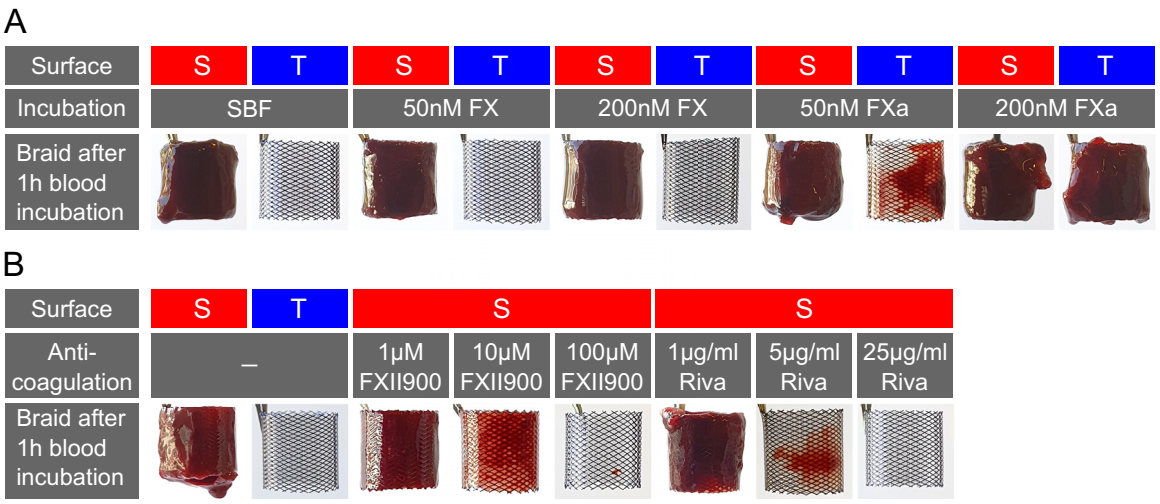

Fig. 5. Influence of (active) coagulation factors FX / FXII on blood clotting. (A) Blood clot formation of standard (S) and treated (T) braids pre-incubated in SBF (control), 50 nM or 200 nM inactive FX or active FXa in SBF. (B) Inhibition of blood clot formation induced by standard surfaces, either by addition of FXII-specific inhibitor FXII900 (1, 10 and 100 nM) or FX-specific inhibitor Rivaroxaban (0, 1, 5 and 25 µg/ml blood).

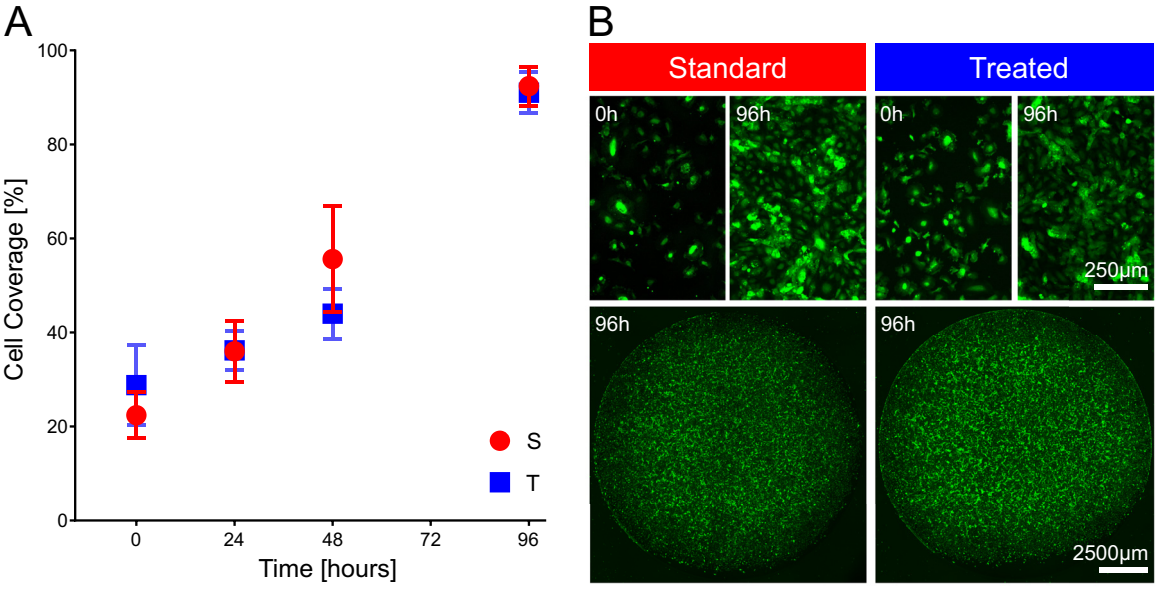

Fig. 6. Endothelialization by HUVECS on standard and treated disks. (A) Cell proliferation over time. Cell coverage data are expressed as average ± standard deviation of 5 independent disks at any given time point. (B) Fluorescence microscopy images showing cell coverage at selected time points. (For interpretation of the references to color in this figure legend, the reader is referred to the web version of this article.)

among all observations: macroscopic thrombus formation, fibrin fiber formation, platelet adhesion, and reduced biomarker concentration of the coagulation cascade and platelet activation. TAT and β-TG evaluations conducted with blood samples from the chandler loop revealed a significantly lower (1 to 2 orders of magnitude) activation of treated versus standard braids and only a marginal, insignificantly higher activation by treated braids when compared to the empty loop ($p = 0.35$ for TAT and $p = 0.94$ for β-TG). These findings suggest a negligible thrombin formation and platelet activation on treated surfaces and also a good apposition of braid and loop wall that did not cause significant hemodynamic turbulences.

4.3. Surface interaction with blood electrolytes

Both treated and standard surfaces showed equivalent oxide layers, consisting almost exclusively of titanium oxide (≥ 97%) with only traces of nickel oxide (Table 1). This is because titanium has higher affinity with oxygen and oxidizes first, confining the nickel in the titanium-depleted (i.e. nickel-rich) metal below the oxide layer [53]; due to the stable oxide layer no significant release of nickel can be expected [54]. Oxygen plasma treatment further oxidized the Nitinol, visualized by slightly increased thickness of the surface oxide layer; this effect potentially improves the barrier properties of the oxide layer resulting in superior corrosion resistance and thus lower nickel release.

The difference between the two surfaces lies in the layer above the surface of the oxide layer: the standard surface is covered by a natural contamination of hydrocarbons originating from the clean room atmosphere. Instead, the hydrophilic treated surface is covered by hydroxides, phosphate groups, calcium, and traces of magnesium ions, which are a consequence of the plasma treatment, phosphate functionalization and subsequent reaction with the double-charged cations present in SBF. Therefore, a similar surface composition can also be expected in contact with blood. This reaction with blood (and SBF) ions takes place also on standard surfaces [53] and is characteristic of titanium alloys, where the

phosphate ions bind to the titanium oxide but maintain a reactivity to calcium ions as well, in contrast e.g. to zirconium where phosphates bind so strongly that they do not further react with calcium ions anymore [55]. However, the reaction is normally slow [56], such that no significant increase of these elements was detected on standard surfaces rinsed with SBF (Suppl. Table 1). Instead, the adsorption of calcium and magnesium is orders of magnitude faster on treated surfaces, where phosphate is already bound on the titanium oxide and the surface is not shielded by the hydrophobic contamination layer. This is supported by the finding that direct immersion of treated devices into blood, without preliminary flushing with a calcium/magnesium-containing solution, led to the same reduction in thrombogenicity response as with flushed samples (Suppl. Fig. 1B). The reaction is probably faster than the adsorption of most blood proteins, also because of the high mobility of small ions compared to the larger proteins. Furthermore, even if these ions are present in low concentrations, they probably affect the Nitinol surface charge and thereby play a critical role in the subsequent adsorption of blood proteins. Since the functionalization is based on titanium oxide, which is naturally present not only on Nitinol but in general on all titanium alloys, due to the high affinity of titanium to oxygen, the same chemical reactions are expected also with pure titanium and other titanium alloys. This expands the range of blood-contacting implants which may benefit from the antithrombogenic effect of this treatment.

4.4. Surface properties steer protein adsorption and activity

Proteins instantly adsorb on foreign surfaces such as braids and stents when they are exposed to blood. Thereby, surface properties steer composition as well as conformation of the adsorbed proteins, which subsequently affect the initiation of coagulation and complement activation. Although many proteins of the coagulation and complement pathway adsorbed on standard and treated surfaces (Suppl. Tables 2 and 3), we observed a reduction of total protein abundance on treated surfaces (Fig. 4A). This is in line with earlier findings on ultra-hydrophilic CoCr surfaces where we observed that hydrophilicity was related to lower protein adsorption [57].

Upstream intrinsic pathway-activating proteins adsorbed with significantly (HMWK, FXI) or insignificantly (FXII, PKK) lower abundance on treated compared to standard surfaces (Fig. 4B). Of note, FXII and FXI in complex with HMWK are known to bind to implant surfaces [58–60]; at this point, the non-enzymatic cofactor HMWK brings FXI and PKK through complexation into close proximity of FXII which can trigger the contact activation cascade (Fig. 7). Thus, the low abundance of all these factors on treated Nitinol could explain the absence of intrinsic coagulation cascade activation, which would result in fibrin fibers and thrombus formation. Additionally, the non-coagulating outcome of treated surfaces in contact with blood could also be regulated by the increased abundance of the FX-inhibitors PROC, PROS and PROZ (Fig. 4C).

On the other hand, the increased abundance of adsorbed extrinsic and common pathway coagulation factors FVII, FX, and (pro) thrombin (FII) on treated Nitinol (Fig. 4C) does not fit well into a model where the coagulation cascade is not activated. It rather indicates that these proteins, dependent on their interaction with the functionalized surface, may remain in their native inactive conformation or lose their potential to get activated and subsequently they cannot contribute to the coagulation cascade. Hydrophobic surfaces, as the standard Nitinol surfaces, probably induce conformational changes of proteins, which upon binding become potent activators. This has been reported for FXII [61], fibrinogen [62], and IgG [63]. It is thought that highly hydrophilic surfaces can avert unfolding and denaturation of adsorbed proteins [45,64–67]. However, conformation as well as activation status of proteins adsorbed to the non-transparent metallic substrates could not be directly measured in this study. Nevertheless, in support of this assumption, we found that pre-adsorption of treated stents with FX could not initiate blood clotting, while pre-adsorption with pre-activated FXa induced a concentration-dependent blood coagulation (Fig. 5A and B). Hence, these results let us conclude that binding on the treated surface did not impair FXa activity, since adsorbed FXa successfully induced blood clotting. Moreover, higher concentrations of FX / FXa did not accelerate coagulation, indicating that adsorbed FX is not a limiting factor in the cascade. Together, these results support the hypothesis that on treated surfaces the majority or totality of adsorbed FX is inactive, while standard surfaces are endowed with FXa. Similarly, native inactive prothrombin rather than active thrombin may have adsorbed on treated surfaces. This assumption is supported by the comparably low TAT concentrations measured in the blood samples that were derived from empty or treated stent-loaded chandler loops (Fig. 3B) and by the absence of fibrin fiber formation, which would be induced by thrombin (Figs. 2 and 3A).

Additionally, the phosphate functionalization of treated surfaces with calcium and magnesium ions in equilibrium with the blood electrolytes seems to steer adsorption of calcium-binding proteins. These include members of the blood coagulation pathway, namely FVII, FX, prothrombin, and the vitamin K-dependent proteins C, S and Z (PROC, PROS and PROZ) (Fig. 7). Interestingly, these proteins are all members of the protein family of vitamin K-dependent proteins, sharing the structural feature of an N-terminal calcium-binding gamma-carboxyglutamic acid-rich (GLA)-domain. Hence, a plausible explanation for the selectivity of these proteins on treated disks could be an interaction of the surface phosphate ions with the GLA-domains mediated by the double-charged calcium cations. Similar GLA-dependent and calcium-mediated interactions have been reported for FX to the phosphate groups of phosphatidylserine [68] and for FVIIa to 1,2-dioleoyl-sn-glycero-3-[phospho-l-serine] (DOPS) lipids [69]. Furthermore, treated surfaces showed significantly reduced adsorption of many proteins involved in complement activation and inflammatory response (Suppl. Table 3). While complement activation can occur via three different pathways (lectin, classical and alternative), foreign surfaces are thought to induce it mainly via the classical and the alternative pathway through complement subcomponent C1q and properdin, respectively [70–72]. The abundance of properdin was significantly reduced on treated surfaces. Additionally, also downstream proteins of the alternative pathway including complement factor H-related proteins 1, 2 and 5 (CFHR1, -2 and -5), and complement factors C3, C5, C6, C7, C8 and C9 were reduced.

Two observations concerning the complement cascade can be done: all significant complement proteins showed reduced adsorption on treated surfaces; activated coagulation pathway is cross-linked with the complement pathway [73]. These findings support a potential increased induction of the alternative complement pathway on standard surfaces, which is instead low or absent on hydrophilic treated surfaces. This may translate in reduced inflammation by treated surfaces.

4.5. Protein layer steers cell adhesion and thrombus formation

Depending on the composition of the adsorbed protein layer, several adverse effects are unleashed. Besides the previously discussed activation of the coagulation and complement cascades, it triggers platelet adhesion and activation, immune response, and inflammation. The reduction of platelet adhesion seen on the ultra-hydrophilic treated surface is in line with similar observations on hydrophilic surfaces in the literature [47,74,75]. The most prominent proteins that promote platelet adhesion on biomaterials are fibrinogen and vWF, due to specific receptors on platelets for these

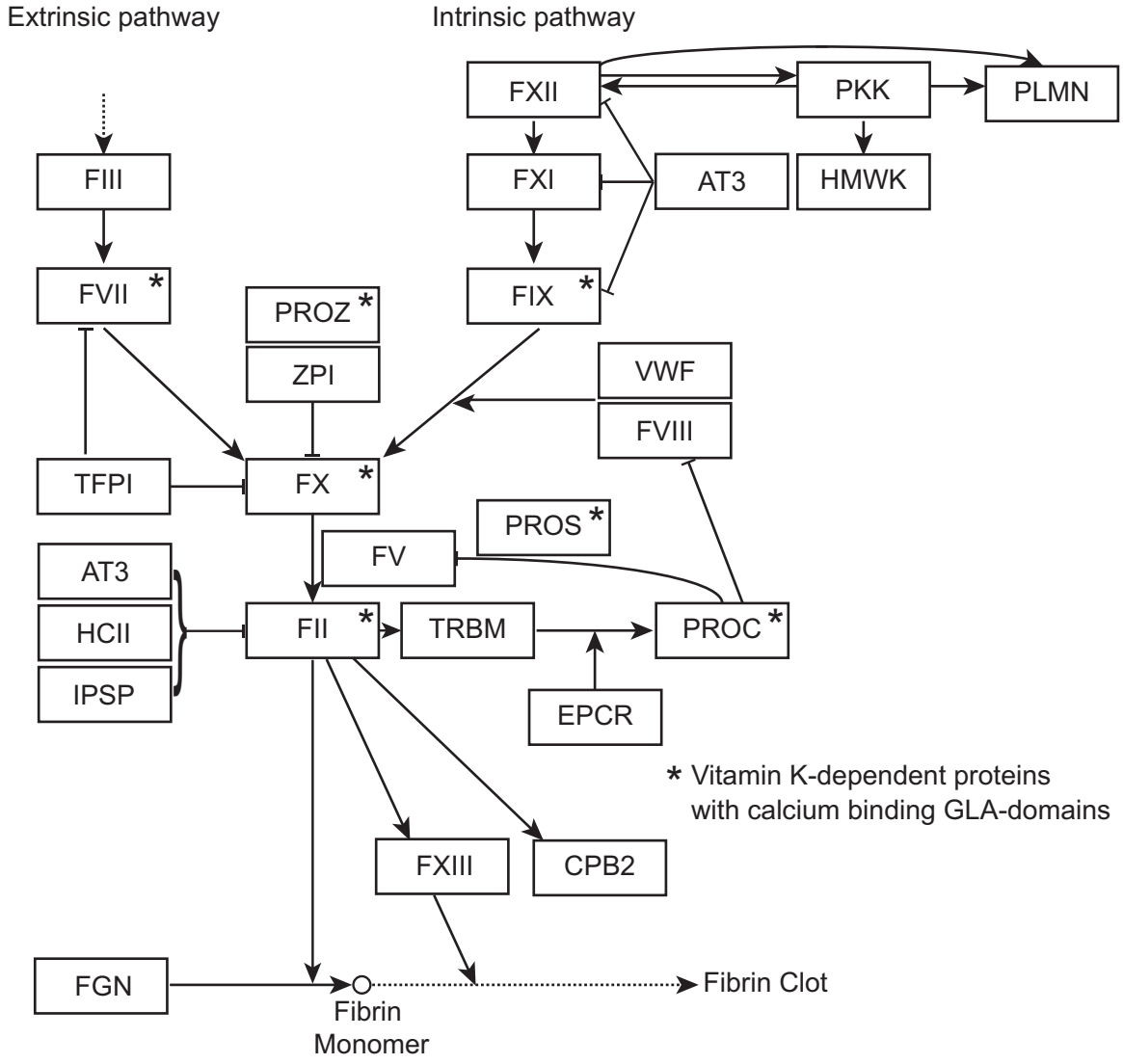

Fig. 7. Blood coagulation cascade. AT3 (antithrombin 3); CPB2 (carboxypeptidase B2); EPCR (endothelial protein C receptor); FII-XIII (coagulation factors II-XII); FGN (fibrinogen); HCII (heparin cofactor 2); HMWK (high molecular weight kininogen); IPSP (plasma serine protease inhibitor); PKK (plasma kallikrein); PLMN (plasminogen); PROC,-S,-Z (vitamin K-dependent proteins C, S and Z); TFPI (tissue factor pathway inhibitor); TRBM (thrombomodulin); vWF (von Willebrand factor); ZPI (protein Z dependent protease inhibitor).

two proteins [45,76]. However, platelet adhesion does not necessarily correlate with the amount of adsorbed fibrinogen and vWF; we already showed on treated CoCr alloys that fibrinogen plays a key role in cell adhesion but acts in a quantity-independent mode [26]. Indeed, adsorption of platelets requires conformational changes of these proteins such that they expose platelet-binding regions. For vWF an active conformation implies shear flow, such that this protein cannot explain the different outcome of static tests; for fibrinogen, nonpolar hydrophobic surfaces tend to induce the greatest degree of unfolding [45,76]. Lower protein denaturation might thus explain why platelet adhesion was reduced on hydrophilic treated surfaces despite non-significant reductions in the amounts of these two proteins.

Like platelets, nucleated cells such as neutrophils and monocytes can adhere and can be activated by proteins adsorbed to the biomaterial. These include fibrinogen, fibronectin and iC3b (reviewed in [77]). Additionally, adhered platelets further trigger activation of nucleated cells. Despite decreased complement protein adsorption and reduced fibrin formation, no significant reduction in the adherence of nucleated cells was observed (Fig. 1); a potential reduction in their activation was not investigated.

4.6. Long-term stability

Long-term stability of the antithrombogenic effect is difficult to assess *in vitro* because of the intrinsic instability of whole blood outside the human body. In this study, the focus was on acute blood response to Nitinol implant surfaces. However, long pre-incubation tests in SBF, which is naturally protein free, indicated that treated surfaces achieve a stable equilibrium with the phosphate and double-charged blood cations. This equilibrium is maintained over the first weeks ($\geq$ 1 month, Suppl. Fig. 1), after which the treated surfaces were still able to steer the adsorption of blood proteins, to avoid their denaturation and to subsequently prevent the activation of the thrombotic cascade. Considering the continuous presence of phosphate and double-charged cations in the blood, we can thus assume that the surface does not become thrombotic within the first weeks even in the presence of proteins. After this critical initial phase, the surface will likely be covered by endothelial cells, which provide a long-lasting antithrombogenic surface [48–52]. Indeed, our *in vitro* observation of an intact endothelialization on treated surfaces (Fig. 6) supports this notion.

Together, we hypothesize that antithrombogenic Nitinol stents for endovascular applications do not necessarily rely on permanent surface coatings. Instead, we propose that the pure hydrophilic metal surface is sufficient, but it requires an initial dynamic equilibrium of the surface with the blood ions prior to protein adsorption. This condition is achieved with the phosphate functionalization.

5. Conclusions

In this study we presented a way to drastically reduce the thrombogenicity of Nitinol by making its surface ultra-hydrophilic and functionalized with phosphate ions. The surface treatment reduced FXII-induced activation of the coagulation cascade and fibrin formation, as well as platelet adhesion and activation. In contrast to standard surfaces, no thrombus formation is observed after 1 h of flow-loop and static human blood tests, even with low concentrations of blood anticoagulant. We propose that the mechanism is mediated by phosphate and calcium ions combined with surface hydrophilicity. This surface leads to a general reduction of protein adsorption, including most proteins of the coagulation or complement cascade, and suggests lower conformational changes of the adsorbed proteins. An exception is represented by the selective adsorption of calcium ion-binding proteins, including the vitamin K-dependent coagulation factors such as FX. Based on FX/FXa pre-adsorption analysis and overall blood-contact outcome we conclude that these proteins, while bound in their active form on standard Nitinol surfaces, are inactive on treated surfaces. Therefore, they do not actively contribute to surface-induced blood coagulation. Thus, this work provides a promising surface treatment for Nitinol-based medical implants to reduce device thrombosis. Since this functionalization is addressed on titanium oxide surfaces, its efficacy can likely be extended to all titanium alloys.

Declaration of Competing Interest

Stefano Buzzi and Arik Zucker are employed by Qvanteq AG, a company performing surface treatments for biomedical devices, which may be considered as potential conflict of interest. All other authors declare that they have no known competing financial interests or personal relationships that could have appeared to influence the work reported in this paper.

Funding

This work was supported by the Swiss Commission for Technology and Innovation (CTI / Innosuisse).

Acknowledgments

Prof. A.R. Studart (Complex Materials, ETH Zürich, Switzerland) is acknowledged for the use of SEM. Christian Heinis and Ganesh Mothukuri (Laboratory of Therapeutic Peptides and Proteins, EPFL, Switzerland) are acknowledged for providing the FXII inhibitor. Armin W. Mäder is acknowledged for constructive discussions.

Data availability

The raw and processed mass spectrometry proteomics data have been deposited to the ProteomeXchange Consortium via the PRIDE [35] partner repository. The data can be accessed with the identifier PXD024284 and is available for download from [https://www.ebi.ac.uk/pride/archive/projects/PXD024284].

Supplementary materials

Supplementary material associated with this article can be found, in the online version, at doi:10.1016/j.actbio.2021.10.022.

References

[1] S. Bauer, P. Schmuki, K. von der Mark, J. Park, Engineering biocompatible implant surfaces, Prog. Mater. Sci. 58 (2013) 261–326, doi:10.1016/j.pmatsci.2012.09.001.
[2] Q. Chen, G.A. Thouas, Metallic implant biomaterials, Mater. Sci. Eng. R Rep. 87 (2015) 1–57, doi:10.1016/j.mser.2014.10.001.
[3] K. Li, C. Wang, J. Yan, Q. Zhang, B. Dang, Z. Wang, Y. Yao, K. Lin, Z. Guo, L. Bi, Y. Han, Evaluation of the osteogenesis and osseointegration of titanium alloys coated with graphene: an *in vivo* study, Sci. Rep. 8 (2018) 1843, doi:10.1038/s41598-018-19742-y.
[4] J. Hong, J. Andersson, K. Nilsson Ekdahl, G. Elgue, N. Axén, R. Larsson, B. Nilsson, Titanium is a highly thrombogenic biomaterial: possible implications for osteogenesis, Thromb. Haemost. 82 (1999) 58–64, doi:10.1055/s-0037-1614630.
[5] V. Milleret, P.S. Lienemann, S. Bauer, M. Ehrbar, Quantitative *in vitro* comparison of the thrombogenicity of commercial dental implants, Clin. Implant Dent. Relat. Res. 21 (2019) 8–14, doi:10.1111/cid.12737.
[6] J.Z. Passer, C.M. Loftus, Postoperative anticoagulation after neurologic surgery, Neurosurg. Clin. N. Am. 29 (2018) 575–583, doi:10.1016/j.nec.2018.06.008.
[7] H. Henkes, P. Bhogal, M. Aguilar Pérez, T. Lenz-Habijan, C. Bannewitz, M. Peters, C. Sengstock, O. Ganslandt, P. Lylyk, H. Monstadt, Anti-thrombogenic coatings for devices in neurointerventional surgery: case report and review of the literature, Interv. Neuroradiol. 25 (2019) 619–627, doi:10.1177/1591019919858000.
[8] M. Broberg, C. Eriksson, H. Nygren, GPIIb/IIIa is the main receptor for initial platelet adhesion to glass and titanium surfaces in contact with whole blood, J. Lab. Clin. Med. 139 (2002) 163–172, doi:10.1067/mlc.2002.121604.
[9] J. Sanchez, G. Elgue, J. Riesenfeld, P. Olsson, Studies of adsorption, activation, and inhibition of factor xii on immobilized heparin, Thromb. Res. 89 (1998) 41–50, doi:10.1016/S0049-3848(97)00310-1.
[10] J. Sánchez, P.B. Lundquist, G. Elgue, R. Larsson, P. Olsson, Measuring the degree of plasma contact activation induced by artificial materials, Thromb. Res. 105 (2002) 407–412, doi:10.1016/S0049-3848(02)00051-8.
[11] G. Tepe, J. Schmehl, H.P Wendel, S. Schaffner, S. Heller, M. Gianotti, C.D Claussen, S.H Duda, Reduced thrombogenicity of nitinol stents-*in vitro* evaluation of different surface modifications and coatings, Biomaterials 27 (2006) 643–650, doi:10.1016/j.biomaterials.2005.06.004.
[12] G. Girdhar, S. Ubl, R. Jahanbekam, S. Thinamany, A. Belu, J. Wainwright, M.F. Wolf, Thrombogenicity assessment of pipeline, pipeline shield, derivo and P64 flow diverters in an *in vitro* pulsatile flow human blood loop model, eNeurologicalSci 14 (2019) 77–84, doi:10.1016/j.ensci.2019.01.004.
[13] G. Cattaneo, C. Bräuner, G. Siekmeyer, A. Ding, S. Bauer, M. Wohlschlögel, L. Lang, T. Hierlemann, M. Akimov, C. Schlensak, A. Schüßler, H.P. Wendel, S. Krajewski, *In vitro* investigation of chemical properties and biocompatibility of neurovascular braided implants, J. Mater. Sci. Mater. Med. (2019) 30, doi:10.1007/s10856-019-6270-6.
[14] M.F. Maitz, M.C.L. Martins, N. Grabow, C. Matschegewski, N. Huang, E.L. Chaikof, M.A. Barbosa, C. Werner, C. Sperling, The blood compatibility challenge. Part 4: Surface modification for hemocompatible materials: Passive and active approaches to guide blood-material interactions, Acta Biomater. 94 (2019) 33–43, doi:10.1016/j.actbio.2019.06.019.
[15] A. Baldwin, J. Belletto, G. Ulrich, Phosphonates and uses therof, WO 2019075261 A1, (2019), https://patentscope.wipo.int/search/en/detail.jsf?docId=WO2019075261. US patent number: US20200239725.
[16] K. Ishihara, H. Oshida, Y. Endo, T. Ueda, A. Watanabe, N. Nakabayashi, Hemocompatibility of human whole blood on polymers with a phospholipid polar group and its mechanism, J. Biomed. Mater. Res. 26 (1992) 1543–1552, doi:10.1002/jbm.820261202.
[17] K. Ishihara, H. Nomura, T. Mihara, K. Kurita, Y. Iwasaki, N. Nakabayashi, Why do phospholipid polymers reduce protein adsorption? J. Biomed. Mater. Res. 39 (1998) 323–330, doi:10.1002/(SICI)1097-4636(199802)39:2⟨323::AID-JBM21⟩3.0.CO;2-C.
[18] D.T.H. Wassell, G. Embery, Adsorption of bovine serum albumin on to titanium powder, Biomaterials 17 (1996) 859–864, doi:10.1016/0142-9612(96)83280-7.
[19] A.P. Valagão Amadeu do Serro, A.C. Fernandes, B. de, J.V. Saramago, W. Norde, Bovine serum albumin adsorption on titania surfaces and its relation to wettability aspects, J. Biomed. Mater. Res. 46 (1999) 376–381, doi:10.1002/(SICI)1097-4636(19990905)46:3⟨376::AID-JBM10⟩3.0.CO;2-T.
[20] H. Sugiyama, T. Hagiwara, H. Watanabe, T. Sakiyama, Effects of ionic substances on the adsorption of egg white proteins to a stainless steel surface, Biosci. Biotechnol. Biochem. 76 (2012) 467–472, doi:10.1271/bbb.110747.
[21] Z. Xu, V.H. Grassian, Bovine serum albumin adsorption on TiO_2 nanoparticle surfaces: effects of pH and coadsorption of phosphate on protein–surface interactions and protein structure, J. Phys. Chem. C 121 (2017) 21763–21771, doi:10.1021/acs.jpcc.7b07525.
[22] J.-L. Yu, R. Andersson, Å. Ljungh, Protein adsorption and bacterial adhesion to biliary stent materials, J. Surg. Res. 62 (1996) 69–73, doi:10.1006/jsre.1996.0175.

[23] E.A. Scott, M.D. Nichols, L.H. Cordova, B.J. George, Y.-S. Jun, D.L. Elbert, Protein adsorption and cell adhesion on nanoscale bioactive coatings formed from poly(ethylene glycol) and albumin microgels, Biomaterials 29 (2008) 4481–4493, doi:10.1016/j.biomaterials.2008.08.003.
[24] P.P. Vicario, Z.J. Lu, I.A. Grigorian, T. Schottman, A lubricious formulation exhibiting reduced thrombogenicity, cell proliferation, and protein adsorption, J. Biomed. Mater. Res. Part B Appl. Biomater. 90B (2009) 452–460, doi:10.1002/jbm.b.31306.
[25] X.M. Li, H.Z. Li, S.P. Wang, H.M. Huang, H.H. Huang, H.J. Ai, J. Xu, MRI-compatible Nb-60Ta-2Zr alloy used for vascular stents: haemocompatibility and its correlation with protein adsorption, Mater. Sci. Eng. C 42 (2014) 385–395, doi:10.1016/j.msec.2014.05.051.
[26] V. Milleret, S. Buzzi, P. Gehrig, A. Ziogas, J. Grossmann, K. Schilcher, A.S. Zinkernagel, A. Zucker, M. Ehrbar, Protein adsorption steers blood contact activation on engineered cobalt chromium alloy oxide layers, Acta Biomater. (2015), doi:10.1016/j.actbio.2015.06.020.
[27] B. Sivaraman, R.A. Latour, The Adherence of platelets to adsorbed albumin by receptor-mediated recognition of binding sites exposed by adsorption-induced unfolding, Biomaterials 31 (2010) 1036–1044, doi:10.1016/j.biomaterials.2009.10.017.
[28] P.J. Cumpson, Angle-resolved X-ray photoelectron spectroscopy, in: D. Briggs, J. Grant (Eds.), X-Ray Photoelectron Spectroscopy, Eds., IM Publications and Surface Spectra Limited, 2003, pp. 651–675.
[29] P.L.J. Gunter, J.W. Niemantsverdriet, Thickness determination of uniform overlayers on rough substrates by angle-dependent XPS, Appl. Surf. Sci. 89 (1995) 69–76, doi:10.1016/0169-4332(95)00014-3.
[30] P.L.J. Gunter, O.L.J. Gijzeman, J.W. Niemantsverdriet, Surface roughness effects in quantitative XPS: magic angle for determining overlayer thickness, Appl. Surf. Sci. 115 (1997) 342–346, doi:10.1016/S0169-4332(97)00007-X.
[31] M. Weber, H. Steinle, S. Golombek, L. Hann, C. Schlensak, H.P. Wendel, M. Avci-Adali, Blood-contacting biomaterials: *in vitro* evaluation of the hemocompatibility, Front. Bioeng. Biotechnol. 6 (2018), doi:10.3389/fbioe.2018.00099.
[32] A.B. Chandler, *In vitro* thrombotic coagulation of the blood; a method for producing a thrombus, Lab. Investig. 7 (1958) 110–114 http://www.ncbi.nlm.nih.gov/pubmed/13540201.
[33] J. Rappsilber, Y. Ishihama, M. Mann, Stop and go extraction tips for matrix-assisted laser desorption/ionization, nanoelectrospray, and LC/MS sample pretreatment in proteomics, Anal. Chem. 75 (2003) 663–670, doi:10.1021/ac026117i.
[34] J. Grossmann, B. Roschitzki, C. Panse, C. Fortes, S. Barkow-Oesterreicher, D. Rutishauser, R. Schlapbach, Implementation and evaluation of relative and absolute quantification in shotgun proteomics with label-free methods, J. Proteom. 73 (2010) 1740–1746, doi:10.1016/j.jprot.2010.05.011.
[35] Y. Perez-Riverol, A. Csordas, J. Bai, M. Bernal-Llinares, S. Hewapathirana, D.J. Kundu, A. Inuganti, J. Griss, G. Mayer, M. Eisenacher, E. Pérez, J. Uszkoreit, J. Pfeuffer, T. Sachsenberg, S. Yilmaz, S. Tiwary, J. Cox, E. Audain, M. Walzer, A.F. Jarnuczak, T. Ternent, A. Brazma, J.A. Vizcaíno, The PRIDE database and related tools and resources in 2019: improving support for quantification data, Nucleic Acids Res. 47 (2019) D442–D450, doi:10.1093/nar/gky1106.
[36] Y. Liao, J. Wang, E.J. Jaehnig, Z. Shi, B. Zhang, Web Gestalt 2019: gene set analysis toolkit with revamped UIs and APIs, Nucleic Acids Res. 47 (2019) W199–W205, doi:10.1093/nar/gkz401.
[37] J. Wilbs, X.D. Kong, S.J. Middendorp, R. Prince, A. Cooke, C.T. Demarest, M.M. Abdelhafez, K. Roberts, N. Umei, P. Gonschorek, C. Lamers, K. Deyle, R. Rieben, K.E. Cook, A. Angelillo-Scherrer, C. Heinis, Cyclic peptide FXII inhibitor provides safe anticoagulation in a thrombosis model and in artificial lungs, Nat. Commun. 11 (2020) 3890, doi:10.1038/s41467-020-17648-w.
[38] J. Schindelin, I. Arganda-Carreras, E. Frise, V. Kaynig, M. Longair, T. Pietzsch, S. Preibisch, C. Rueden, S. Saalfeld, B. Schmid, J.-Y. Tinevez, D.J. White, V. Hartenstein, K. Eliceiri, P. Tomancak, A. Cardona, Fiji: an open-source platform for biological-image analysis, Nat. Methods 9 (2012) 676–682, doi:10.1038/nmeth.2019.
[39] M. Bohner, Calcium orthophosphates in medicine: from ceramics to calcium phosphate cements, Injury 31 (2000) D37–D47, doi:10.1016/S0020-1383(00)80022-4.
[40] T. Hanawa, M. Ota, Calcium phosphate naturally formed on titanium in electrolyte solution, Biomaterials 12 (1991) 767–774, doi:10.1016/0142-9612(91)90028-9.
[41] L. Frauchiger, M. Taborelli, B.O. Aronsson, P. Descouts, Ion adsorption on titanium surfaces exposed to a physiological solution, Appl. Surf. Sci. 143 (1999) 67–77, doi:10.1016/S0169-4332(98)00932-5.
[42] K.E. Brummel, S. Butenas, K.G. Mann, An integrated study of fibrinogen during blood coagulation, J. Biol. Chem. 274 (1999) 22862–22870, doi:10.1074/jbc.274.32.22862.
[43] K.E. Brummel, S.G. Paradis, S. Butenas, K.G. Mann, Thrombin functions during tissue factor-induced blood coagulation, Blood 100 (2002) 148–152, doi:10.1182/blood.V100.1.148.
[44] S.L. Hirsh, D.R. McKenzie, N.J. Nosworthy, J.A. Denman, O.U. Sezerman, M.M.M. Bilek, The Vroman effect: competitive protein exchange with dynamic multilayer protein aggregates, Colloids Surf. B Biointerfaces 103 (2013) 395–404, doi:10.1016/j.colsurfb.2012.10.039.
[45] J.L. Brash, T.A. Horbett, R.A. Latour, P. Tengvall, The blood compatibility challenge. Part 2: protein adsorption phenomena governing blood reactivity, Acta Biomater. 94 (2019) 11–24, doi:10.1016/j.actbio.2019.06.022.
[46] L. Vroman, A.L. Adams, Identification of rapid changes at plasma-solid interfaces, J. Biomed. Mater. Res. 3 (1969) 43–67, doi:10.1002/jbm.820030106.
[47] V. Milleret, A. Ziogas, S. Buzzi, R. Heuberger, A. Zucker, M. Ehrbar, Effect of oxide layer modification of CoCr stent alloys on blood activation and endothelial behavior, J. Biomed. Mater. Res. Part B Appl. Biomater. 103 (2015) 629–640, doi:10.1002/jbm.b.33232.
[48] R. Kadirvel, Y.-H. Ding, D. Dai, I. Rezek, D.A. Lewis, D.F. Kallmes, Cellular mechanisms of aneurysm occlusion after treatment with a flow diverter, Radiology 270 (2014) 394–399, doi:10.1148/radiol.13130796.
[49] W. Brinjikji, D.F. Kallmes, R. Kadirvel, Mechanisms of healing in coiled intracranial aneurysms: a review of the literature, Am. J. Neuroradiol. 36 (2015) 1216–1222, doi:10.3174/ajnr.A4175.
[50] K. Ravindran, M.M. Salem, A.Y. Alturki, A.J. Thomas, C.S. Ogilvy, J.M. Moore, Endothelialization following flow diversion for intracranial aneurysms: a systematic review, Am. J. Neuroradiol. 40 (2019) 295–301, doi:10.3174/ajnr.A5955.
[51] W. Zheng, Z. Wang, L. Song, Q. Zhao, J. Zhang, D. Li, S. Wang, J. Han, X.-L. Zheng, Z. Yang, D. Kong, Endothelialization and patency of RGD-functionalized vascular grafts in a rabbit carotid artery model, Biomaterials 33 (2012) 2880–2891, doi:10.1016/j.biomaterials.2011.12.047.
[52] G. De Visscher, L. Mesure, B. Meuris, A. Ivanova, W. Flameng, Improved endothelialization and reduced thrombosis by coating a synthetic vascular graft with fibronectin and stem cell homing factor SDF-1α, Acta Biomater. 8 (2012) 1330–1338, doi:10.1016/j.actbio.2011.09.016.
[53] T. Hanawa, S. Hiromoto, K. Asami, O. Okuno, K. Asaoka, Surface oxide films on titanium alloys regenerated in Hanks' solution, Mater. Trans. 43 (2002) 3000–3004, doi:10.2320/matertrans.43.3000.
[54] S.J.L. Sullivan, M.L. Dreher, J. Zheng, L. Chen, D. Madamba, K. Miyashiro, C. Trépanier, S. Nagaraja, Effects of oxide layer composition and radial compression on nickel release in Nitinol stents, Shape Mem. Superelast. 1 (2015) 319–327, doi:10.1007/s40830-015-0028-x.
[55] Y. Tsutsumi, D. Nishimura, H. Doi, N. Nomura, T. Hanawa, Difference in surface reactions between titanium and zirconium in Hanks ' solution to elucidate mechanism of calcium phosphate formation on titanium using XPS and cathodic polarization, Mater. Sci. Eng. C 29 (2009) 1702–1708, doi:10.1016/j.msec.2009.01.016.
[56] A. Hiji, T. Hanawa, M. Shimabukuro, P. Chen, M. Ashida, K. Ishikawa, Initial formation kinetics of calcium phosphate on titanium in Hanks' solution characterized using XPS, Surf. Interface Anal. 53 (2021) 185–193, doi:10.1002/sia.6900.
[57] V. Milleret, A. Ziogas, S. Buzzi, R. Heuberger, A. Zucker, M. Ehrbar, Effect of oxide layer modification of CoCr stent alloys on blood activation and endothelial behavior, J. Biomed. Mater. Res. Part B Appl. Biomater. 103 (2015) 629–640, doi:10.1002/jbm.b.33232.
[58] C.F. Scott, L.D. Silver, M. Schapira, R.W. Colman, Cleavage of human high molecular weight kininogen markedly enhances its coagulant activity. Evidence that this molecule exists as a procofactor, J. Clin. Investig. 73 (1984) 954–962, doi:10.1172/JCI111319.
[59] E.A. Vogler, C.A. Siedlecki, Contact activation of blood-plasma coagulation, Biomaterials 30 (2009) 1857–1869, doi:10.1016/j.biomaterials.2008.12.041.
[60] R.S. Woodruff, B. Sullenger, R.C. Becker, The many faces of the contact pathway and their role in thrombosis, J. Thromb. Thrombolysis 32 (2011) 9–20, doi:10.1007/s11239-011-0578-5.
[61] I. Schousboe, B.T. Nystrøm, G.H. Hansen, Differential binding of factor XII and activated factor XII to soluble and immobilized fibronectin - localization of the Hep-1/Fib-1 binding site for activated factor XII, FEBS J. 275 (2008) 5161–5172, doi:10.1111/j.1742-4658.2008.06647.x.
[62] Y. Wu, F.I. Simonovsky, B.D. Ratner, T.A. Horbett, The role of adsorbed fibrinogen in platelet adhesion to polyurethane surfaces: a comparison of surface hydrophobicity, protein adsorption, monoclonal antibody binding, and platelet adhesion, J. Biomed. Mater. Res. A 74 (2005) 722–738, doi:10.1002/jbm.a.30381.
[63] P. Tengvall, A. Askendal, I. Lundström, Ellipsometric *in vitro* studies on the activation of complement by human immunoglobulins M and G after adsorption to methylated silicon, Colloids Surf. B Biointerfaces 20 (2001) 51–62, doi:10.1016/S0927-7765(00)00174-0.
[64] C.A. Siedlecki, R.E. Marchant, Atomic force microscopy for characterization of the biomaterial interface, Biomaterials 19 (1998) 441–454, doi:10.1016/S0142-9612(97)00222-6.
[65] R.A. Latour, Biomaterials: Protein-Surface Interactions, 2nd ed., Informa Healthcare, New York, NY, 2008, doi:10.1201/9780429154065.
[66] T. Horbett, J.L. Brash, W. Norde, Proteins at Interfaces III State of the Art 2012, American Chemical Society, Washington, DC, 2012, doi:10.1021/bk-2012-1120.
[67] A.A. Thyparambil, Y. Wei, R.A. Latour, Experimental characterization of adsorbed protein orientation, conformation, and bioactivity, Biointerphases 10 (2015) 019002, doi:10.1116/1.4906485.
[68] M.P. Muller, Y. Wang, J.H. Morrissey, E. Tajkhorshid, Lipid specificity of the membrane binding domain of coagulation factor X, J. Thromb. Haemost. 15 (2017) 2005–2016, doi:10.1111/jth.13788.
[69] Y.Z. Ohkubo, E. Tajkhorshid, Distinct structural and adhesive roles of Ca^{2+} in membrane binding of blood coagulation factors, Structure 16 (2008) 72–81, doi:10.1016/j.str.2007.10.021.
[70] B. Nilsson, K.N. Ekdahl, T.E. Mollnes, J.D. Lambris, The role of complement in biomaterial-induced inflammation, Mol. Immunol. 44 (2007) 82–94, doi:10.1016/j.molimm.2006.06.020.

[71] A.E. Engberg, J.P. Rosengren-Holmberg, H. Chen, B. Nilsson, J.D. Lambris, I.A. Nicholls, K.N. Ekdahl, Blood protein-polymer adsorption: Implications for understanding complement-mediated hemoincompatibility, J. Biomed. Mater. Res. Part A 97A (2011) 74–84, doi:10.1002/jbm.a.33030.
[72] K.N. Ekdahl, J.D. Lambris, H. Elwing, D. Ricklin, P.H. Nilsson, Y. Teramura, I.A. Nicholls, B. Nilsson, Innate immunity activation on biomaterial surfaces: a mechanistic model and coping strategies, Adv. Drug Deliv. Rev. 63 (2011) 1042–1050, doi:10.1016/j.addr.2011.06.012.
[73] K. Oikonomopoulou, D. Ricklin, P.A. Ward, J.D. Lambris, Interactions between coagulation and complement-their role in inflammation, Semin. Immunopathol. 34 (2012) 151–165, doi:10.1007/s00281-011-0280-x.
[74] S. Takemoto, T. Yamamoto, K. Tsuru, S. Hayakawa, A. Osaka, Platelet adhesion on metal oxide layers, Key Eng. Mater. 254-256 (2004) 853–856, doi:10.4028/www.scientific.net/kem.254-256.853.
[75] A.W. Tulloch, Y. Chun, D.S. Levi, K.P. Mohanchandra, G.P. Carman, P.F. Lawrence, D.A. Rigberg, Super hydrophilic thin film nitinol demonstrates reduced platelet adhesion compared with commercially available endograft materials, J. Surg. Res. 171 (2011) 317–322, doi:10.1016/j.jss.2010.01.014.
[76] T.A. Horbett, Fibrinogen adsorption to biomaterials, J. Biomed. Mater. Res. Part A 106 (2018) 2777–2788, doi:10.1002/jbm.a.36460.
[77] M.B. Gorbet, M.V. Sefton, Biomaterial-associated thrombosis: roles of coagulation factors, complement, platelets and leukocytes, Biomaterials 25 (2004) 5681–5703, doi:10.1016/j.biomaterials.2004.01.023.